# High-Resolution ISAR Imaging for High-Speed Targets via Joint Intra-Pulse and Inter-Pulse Translational Motion Compensation

Jiabao Wang [1], Shuai Shao* [1] and Jiaqi Wei [2]
[1] National Key Laboratory of Radar Signal Processing, Xidian University, Xi'an, China
E-mail: jiabaowang@stu.xidian.edu.cn, sshao@xidian.edu.cn(*: Corresponding author)
[2] The School of Information Science and Technology, Northwest University, Xi'an, China
E-mail: weijiaqi@nwu.edu.cn

***Abstract*— High-resolution inverse synthetic aperture radar (ISAR) imaging technology is a key method for achieving situational awareness and precise recognition of high-speed moving targets. However, the high-speed movement of targets can cause intra-pulse and inter-pulse translational motion errors, resulting in severe defocusing of ISAR images. To address this issue, this paper proposes an algorithm for high-resolution ISAR imaging of high-speed targets via joint intra-pulse and inter-pulse translational motion compensation (JIPMC). This algorithm utilizes an improved matched filter to achieve precise pulse compression, effectively eliminating intra-pulse motion errors. Based on the homogeneity of intra-pulse and inter-pulse translational motion errors, this paper constructs an intra-pulse and inter-pulse translational motion error model. Combined with optimal parameter estimation, it achieves joint correction of intra-pulse and inter-pulse translational motion errors. The proposed algorithm avoids the cascaded processing of intra-pulse motion compensation (IPMC), envelope alignment, and initial phase correction, significantly reducing error propagation and improving the accuracy and robustness of motion compensation. For optimal parameter estimation, the proposed algorithm utilizes the artificial bee colony (ABC) algorithm to solve the optimization problem under the minimum entropy criterion. The ABC algorithm combines global search and local optimization capabilities, thereby effectively guaranteeing the global optimality of the solution. Experimental results validate the effectiveness and robustness of the proposed method for high-resolution ISAR imaging of high-speed targets.**

## I. INTRODUCTION

Inverse synthetic aperture radar (ISAR) simulates the effect of a large-aperture antenna by utilizing the relative motion between the target and the radar. Combined with motion compensation technology, it achieves high-resolution two-dimensional imaging of non-cooperative moving targets [1],[2], featuring advantages such as all-day, all-weather capability and high resolution. In recent years, aerospace science and technology has developed rapidly worldwide, giving rise to a series of aerospace targets with high-speed characteristics, including fifth-generation fighter jets, guided missiles, and various space vehicles. With its excellent high-resolution imaging detection performance for high-speed targets and strong target feature extraction and analysis capabilities, ISAR occupies a key position in the field of modern aerospace situation awareness and target recognition [3],[4]. However, due to the high-speed characteristics of aerospace targets and the low signal-to-noise ratio (SNR) environment, the intra-pulse motion in target echoes cannot be ignored. Meanwhile, the low SNR environment also poses great challenges for translational motion compensation. Therefore, the research on high-resolution ISAR imaging algorithms for high-speed targets is of practical significance for target recognition and space situation awareness.

In the ISAR imaging process, target motion can be divided into translational motion and rotational motion. The rotational motion causes each scattering point on the target to exhibit different doppler frequencies, serving as the basis for achieving high azimuth resolution. The translational motion, which is the overall motion of the target along the radar line-of-sight (RLOS), makes the scattering points on the target generate the same doppler frequency. It not only contributes nothing to imaging but also leads to envelope walk and initial phase errors. Translational motion compensation is typically performed in a hierarchical manner, that is, envelope alignment is first carried out, followed by initial phase correction. Due to the non-cooperative nature of the target, envelope alignment is usually achieved by leveraging the similarity of adjacent range profiles, such as the cross-correlation method [5] and the minimum entropy method [6]. The commonly used methods for initial phase correction are mainly divided into two categories: the prominent point phase tracking method [7] and the image index method [8]. Since the above algorithms belong to cascaded translational motion compensation, they often cause error propagation, leading to compensation failure under low signal-to-noise ratio conditions. Meanwhile, for high-speed targets, the

979-8-3315-7206-8/25/$31.00 

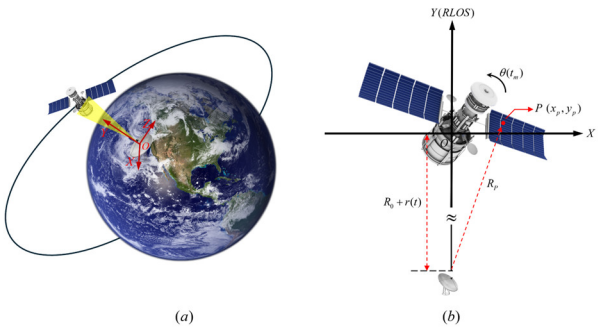


Fig. 1. ISAR geometry
(a) 3D geometry, (b) Simplified 2D geometry.

"stop and go" echo model is no longer applicable [9],[10]. Therefore, intra-pulse motion compensation (IPMC) must be performed before translational motion compensation. If cascaded translational motion compensation (CTMC) is still used, there will be three cascaded steps, which will lead to further error propagation and amplification in the cascaded processing, introducing more errors into the subsequent azimuth dimension focusing processing.

To address the aforementioned issues, this paper proposes a high-resolution ISAR imaging algorithm for high-speed targets via joint intra-pulse and inter-pulse motion compensation (JIPMC). First, a high-speed target echo signal model is established. Then, an IPMC method based on a reconstructed matched filter is proposed. This method is further integrated with the joint translational motion compensation (JTMC) algorithm [11] to form a unified compensation framework. Moreover, the artificial bee colony (ABC) algorithm [12] is employed to estimate motion parameters. Through this approach, high-resolution ISAR imaging for high-speed targets is effectively achieved. The ABC algorithm, as a swarm intelligence optimization method inspired by the foraging behavior of honey bees, exhibits distinct advantages over other swarm intelligence algorithms such as particle swarm optimization (PSO) [13] and genetic algorithm (GA) [14]. Its strengths lie in the collaborative mechanism among three types of bees, which enables a balanced integration of global exploration and local exploitation during the search process. Featuring a simple algorithmic structure, the ABC algorithm adaptively adjusts its search strategies to enhance adaptability to complex nonlinear problems. Extensive simulation experiments validate the effectiveness and robustness of the proposed method in high-resolution ISAR imaging of high-speed targets.

## II. SIGNAL MODEL

Fig.1(a) demonstrates the 3D geometry of ISAR imaging. Since the result of ISAR imaging is a two-dimensional projection of a three-dimensional object on the radar imaging plane, the motion relationship between the target and the radar can be represented by the 2D geometry shown in Fig.1(b). In Fig.1(b), $R_0$ denotes the initial distance between the radar and the target, and $r(t)$ represents the instantaneous radial distance variation caused by the target's translational motion. XOY plane represents the imaging projection plane (IPP), where the Y-axis coincides with the RLOS and represents the range dimension; the X-axis represents the azimuth dimension; and the origin O coincides with the equivalent rotation center of the target. According to the geometric relationship, the instantaneous distance between the radar and the scattering point $p$ on the target can be expressed as:

$$R_p(t;t_m) \approx R_0 + r(t) + x_p \sin\left(\theta(t_m)\right) + y_p \cos\left(\theta(t_m)\right) \quad (1)$$

Where $t_m$ stands for the slow time, $t = \hat{t} + t_m$ the total time, $\hat{t} \in \left[-T_p/2, T_p/2\right]$ the fast time, and $\theta(t_m)$ signifies the rotation angle of the target within the $t_m$ time. In this paper, the radar transmits a linear frequency modulation (LFM) signal, which is expressed as follows:

$$s(\hat{t};t_m) = rect\left[\frac{\hat{t}}{T_p}\right] \cdot \exp\left(j2\pi f_c t + j\pi\gamma\hat{t}^2\right) \quad (2)$$

Where $T_p$ represents the pulse width, $f_c$ is the carrier frequency, $\gamma = B/T_p$ denotes the chirp rate of the LFM signal, and $B$ signifies the signal bandwidth. Due to the high-speed motion of the target, the "stop and go" echo model is no longer applicable, meaning that the translational motion of the target during the pulse duration needs to be considered. Assuming that the radial motion of the target within the coherent processing interval (CPI) is a uniformly accelerated motion with a radial velocity of $v_r$ and a radial acceleration of $a_r$, and the target is in a stable flight phase where the radial acceleration $a_r$ is small, thus its influence on intra-pulse motion is ignored. Equation (1) can be further expressed as:

$$R_p(\hat{t};t_m) = R_r(t_m) + v_r\hat{t} + \Delta R_S(t_m) \quad (3)$$

Where $r(t_m) = v_r t_m + (1/2)a_r t_m^2$ represents the translational motion distance of the target at time $t_m$, $R_r(t_m) = R_0 + r(t_m)$ is the instantaneous radial distance between the target center and the radar at time $t_m$, and $\Delta R_S(t_m) = \sin\left(\theta(t_m)\right) + y_p\cos\left(\theta(t_m)\right)$ represents the instantaneous distance variation caused by the target's rotational motion, the echo signal of the scattering point $p$ can be expressed as:

$$s_p(\hat{t};t_m) = \text{rect}\left[\frac{\hat{t} - \tau(\hat{t};t_m)}{T_p}\right] \cdot \exp\left\{\begin{matrix} j2\pi f_c\left[\hat{t} - \tau(\hat{t};t_m)\right] \\ +j\pi\gamma\left[\hat{t} - \tau(\hat{t};t_m)\right]^2 \end{matrix}\right\} \quad (4)$$

Where $\tau(\hat{t};t_m)=2R_p(\hat{t};t_m)/c$ , and $c$ represents the light velocity. Let $\alpha=(1-2v_r/c)$ , which is called the intra-pulse motion error factor. Assuming there are P scattering points on the target, the total echo signal of the target can be expressed as:

$$S(\hat{t};t_m)=\sum_{p=1}^{P}\left\{\sigma_p \mathrm{rect}\left[\frac{\alpha\hat{t}-\tau'(t_m)}{T_p}\right]\cdot\exp\left\{\begin{matrix}j2\pi f_c\left[\alpha\hat{t}-\tau'(t_m)\right]\\+j\pi\gamma\left[\alpha\hat{t}-\tau'(t_m)\right]^2\end{matrix}\right\}\right\} \tag{5}$$

where $\tau'(t_m)=2\left[R_r(t_m)+\Delta R_S(t_m)\right]/c$ , $\sigma_p$ represents the backscattering coefficient of the scattering point p. The above echo model takes into account intra-pulse motion. Compared with the "stop-and-go" echo model, $\alpha$ will lead to the broadening of the main lobe width and the significant increase of the integral side lobe ratio (ISLR) after pulse compression. The time-frequency coupling effect can also lead to a positional shift in the high-resolution range profile (HRRP) and cause distortion of the focus in the azimuth dimension. Therefore, IPMC must be carried out. In the third section of this paper, the JIPMC algorithm will be introduced.

## III. Joint Intra-pulse and Inter-pulse Translational Motion Compensation Algorithm

### A. Processing Flow of JIPMC

The signal model in section 2 considers intra-pulse motion. Due to the influence of $\alpha$ , if traditional matched filtering is directly applied to (5), a "mismatch" phenomenon will occur. Therefore, it is necessary to improve the matched filter to achieve accurate pulse compression of (5), allowing the matched filtering process to both eliminate intra-pulse motion errors and accomplish pulse compression. The new matched filter function can be expressed as:

$$h_{v_r}(\hat{t})=rect\left[\frac{\alpha\hat{t}}{T_p}\right]\exp\left\{-j\pi\gamma(\alpha\hat{t}-\frac{2R_{ref}}{c})^2\right\} \tag{6}$$

Where $R_{ref}=R_0$ is the reference distance. At the same time, in order to eliminate the influence of the extra term in the phase, the reference carrier frequency when removing the carrier frequency should be modified to $f_c'=\alpha f_c$ , After carrier frequency removal and frequency-domain matched filtering, (5) can be expressed in the range-frequency domain as follows:

$$S(f;t_m)\approx\sum_{p=1}^{P}\sigma_p rect\left[\frac{f}{\alpha B}\right]\exp\left\{\frac{-4\pi(f/\alpha+f_c)}{c}\left\{\begin{matrix}r(t_m)\\+\Delta R_S(t_m)\end{matrix}\right\}\right\} \tag{7}$$

The following JTMC term is thus constructed:

$$C_{v_r,a_r}(f,t_m)=\exp\left\{\frac{4\pi(f/\alpha+f_c)}{c}r(t_m)\right\} \tag{8}$$

By multiplying (7) with (8) and then applying an inverse fast Fourier transform (IFFT) along the range dimension, we obtain:

$$S(\hat{t};t_m)=\sum_{p=1}^{P}\sigma_p \sin c[B(\alpha\hat{t}-\frac{2\Delta R_S(t_m)}{c})]\cdot\exp\left\{-j\frac{4\pi}{\lambda}\Delta R_S(t_m)\right\} \tag{9}$$

Equation (9) eliminates the intra-pulse motion errors and achieves high-precision translational compensation through JTMC. Since we assume stable target flight in Section 2, standard azimuth focusing can subsequently be performed to obtain a high-quality ISAR image. However, the aforementioned algorithm assumes that the target motion parameters are known, which is generally not the case in practice. Therefore, in the following subsection, we introduce an optimal parameter estimation method based on the ABC algorithm.

### B. Establish Optimization Function

Before performing optimal parameter estimation, we first need to establish optimization function. Let $*_F$ denote frequency-domain pulse compression, then (5) after JIPMC can be expressed as:

$$g=IFFT_{\hat{t}}\left[S*_F h_{v_r}\cdot C_{v_r,a_r}\right] \tag{10}$$

Where $IFFT_{\hat{t}}$ indicates IFFT in the range dimension. Since the target is in a stable state of motion, performing a fast Fourier transform (FFT) on (10) in the azimuth dimension can yield a high-resolution ISAR image:

$$I=FFT_{t_m}\left[g\right] \tag{11}$$

Image entropy is commonly used to measure the focusing effect of an image. The smaller the image entropy, the better the focusing performance of the image. Therefore, image entropy is used as an optimization function, and the target motion parameters can be obtained by solving the following minimum entropy optimization problem:

$$\left\langle\hat{v}_r,\hat{a}_r\right\rangle=\arg\min_{\hat{v}_r,\hat{a}_r}\left\{IE(I)\right\} \tag{12}$$

Where *IE* represents the calculation of the image entropy value. For an ISAR image $I$ with $N$ range cells and $M$ Doppler cells, the calculation formula for its entropy is as follows:

$$IE=\sum_{m=0}^{M-1}\sum_{n=0}^{N-1}\frac{\left|I(n,m)\right|^2}{E}\ln\frac{\left|I(n,m)\right|^2}{E} \tag{13}$$

Where $E=\sum_{m=0}^{M-1}\sum_{n=0}^{N-1}\left|I(n,m)\right|^2$ denotes the signal energy. The optimal parameter estimation based on the ABC algorithm will be introduced in the next subsection.

### C. Optimal Parameter Estimation via ABC Algorithm

The basic idea of the ABC algorithm is to simulate the foraging behavior of bees, which are divided into three types of bee roles: employed bees, onlooker bees and scout bees. Both employed bees and onlooker bees account for half of the bee colony, and their quantity is equal to the number of nectar sources. Optimization is achieved through the collaboration of the three types of bee roles. For the objective function:

$$\min IE\left\{I(v_r, a_r)\right\} \tag{14}$$

Let $X = [v_r, a_r]$ be denoted as a two-dimensional solution vector. The detailed steps of the algorithm are as follows:

Step1: Initialization: Set the number of nectar sources N, the number of iterations $u = 1$, the maximum number of iterations $u_{\max}$ and the abandonment threshold $T_{\text{limit}}$. Define the i-th nectar source location as $X_i = [x_{i1}, x_{i2} \cdots x_{iM}]$, where M is the dimension of the solution space. The initial positions are generated according to the following equation:

$$X_i = X_{low} + \text{rand} \cdot (X_{high} - X_{low}) \tag{15}$$

where $X_{low}$ and $X_{high}$ are the lower and upper bounds of the solution space respectively, and *rand* denotes a random number generation function that can produce random numbers between 0 and 1.

Step2: Fitness calculation: To convert the minimization problem into a maximization problem (simulating nectar concentration), define the fitness function as follows:

$$fit(i) = \frac{1}{1 + IE\left\{I(X_i)\right\}} \tag{16}$$

Step3: Employed bee phase: Each employed bee randomly selects a neighboring solution $x_{kj}$ in a dimension $j$. If $fit(k) > fit(i)$, the position of the solution is updated. The update formula is as follows:

$$x_{ij}^{new} = x_{ij} + \phi \cdot (x_{ij} - x_{kj}) \tag{17}$$

where $\phi \in [-1,1]$ is a random perturbation factor. The new solution position after updating is denoted as $X_i^{new}$, and the corresponding fitness is calculated according to (16). When the fitness of $X_i^{new}$ is better than that of $X_i$, a greedy selection method is adopted to replace $X_i$ with $X_i^{new}$, otherwise, $X_i$ is retained. After all employed bees complete the calculation, they share the fitness information with onlooker bees.

Step4: Onlooker bee phase: Onlooker bees calculate the selection probability based on the fitness information transmitted by employed bees. The calculation formula is as follows:

$$p_i = \frac{fit(i)}{\sum_{k=1}^{N} fit(k)} \tag{18}$$

The larger the probability $p_i$, the higher the possibility that the solution $X_i$ is selected. After the onlooker bee selects the solution $X_i$, it generates a new nectar source around the nectar source $X_i$ according to (17), and determines the retained nectar source in the same way as the employed bees.

Step5: Scout bee phase: If a solution $X_i$ remains unchanged for $T_{\text{limit}}$ consecutive times, it is regarded as a "barren nectar source", and a scout bee randomly generates a new solution according to (15) to replace it.

Step6: Termination condition: Let $u = u + 1$, if $u = u_{\max}$ terminate the loop; otherwise, return to Step 3.

## IV. Results and Analysis

The purpose of this section is to verify the effectiveness of the proposed algorithm. The simulation model is shown in Fig.2, and the simulation parameters are listed in TABLE I. In the simulation, comparative experiments between the proposed algorithm, JTMC, and IPMC+CTMC are set up to verify the superiority of the proposed algorithm.

TABLE I. Main Simulation Parameter

| Parameters | Values |
|---|---|
| Carrier frequency | 10GHz |
| Bandwidth | 500MHz |
| Pulse duration | 2us |
| Sampling frequency | 520MHz |
| PRF | 1024Hz |

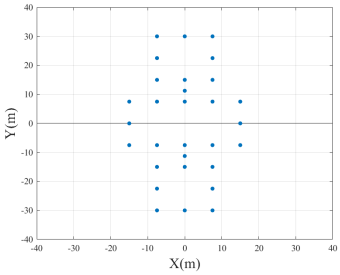


Fig. 2. Scattering point model of satellite

The first three columns in Fig.3 show the ISAR imaging results and corresponding image entropy of the three algorithms under different velocity parameters. It can be seen that the proposed algorithm consistently outperforms the other two algorithms at different velocities. From the convergence curve and estimation results in the fourth column of the figure, it can be seen that after about 25 iterations, the image entropy value tends to remain unchanged and the estimation results are highly accurate, indicating that the optimization algorithm has good accuracy and convergence. Fig.4 shows the comparison results

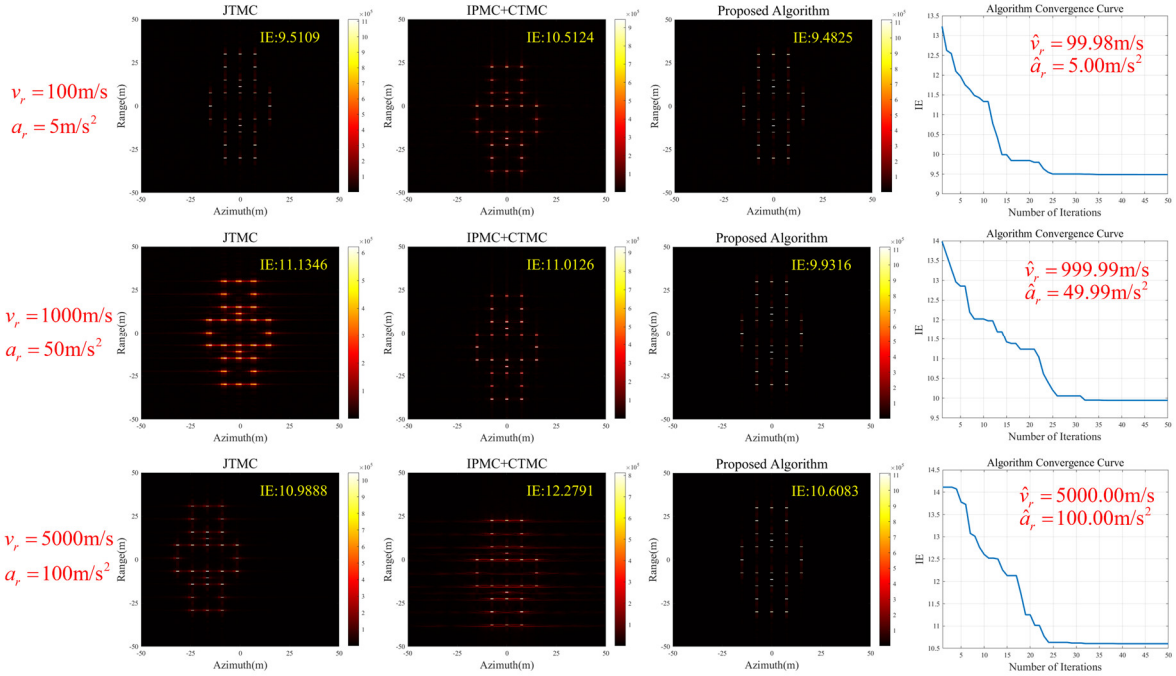


Fig. 3. Comparison results of algorithms at different speeds (SNR=0dB)

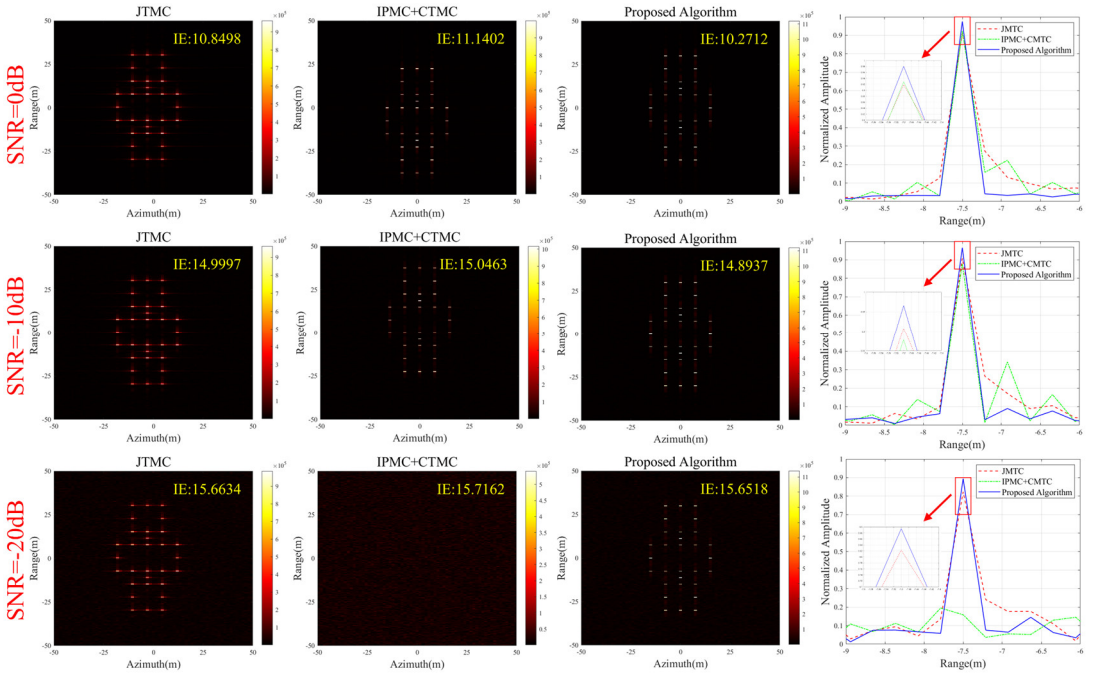


Fig. 4. Comparison results of algorithms at different SNR ( $v_r$=2000m/s,$a_r$=60m/s$^2$ )

of the algorithms under different SNR. The proposed algorithm consistently outperforms the other two algorithms at different SNR, verifying the robustness of the proposed algorithm under low SNR conditions. The fourth column in Fig.4 also shows the local HRRP of the three algorithms after range alignment. It can be seen that the proposed algorithm effectively eliminates the main lobe broadening and ISLR increasing phenomena caused by intra-pulse motion errors compared to the other two algorithms.

In summary, the simulation experiments validate the effectiveness and robustness of the algorithm for high-resolution ISAR imaging of high-speed targets.

## V. CONCLUSIONS

This paper proposes a high-resolution ISAR imaging algorithm for high-speed targets based on JIPMC. First, a high-speed target echo model is established. Then, by integrating the IPMC algorithm with the JTMC algorithm and incorporating optimal parameter estimation based on the ABC algorithm, joint processing is achieved. Finally, simulation and comparative experiments demonstrate the effectiveness and robustness of the proposed algorithm for high-resolution ISAR imaging of high-speed targets.

## VI. ACKNOWLEDGMENT

This work was supported by the Foundation of National Key Laboratory of Radar Signal Processing under Grant JKW202305, the China Postdoctoral Science Foundation under Grant 2022M722502, the Shaanxi Postdoctoral Sustentation Fund with grant number 2023BSHYDZZ94, the Fundamental Research Funds for the Central Universities with grant number ZYTS25143, the Aeronautical Science Foundation of China, and the National Key Lab of Microwave Imaging Technology.

## REFERENCES

[1] H.-Y. Fan, L. Ren, E. Mao, and Q. Liu, "A High-Precision Method of Phase-Derived Velocity Measurement and Its Application in Motion Compensation of ISAR Imaging," IEEE Transactions on Geoscience and Remote Sensing, vol. 56, no. 1, pp. 60–77, Jan. 2018.

[2] S. Shao, H. Liu, L. Zhang, P. Wang, and J. Wei, "Ultrawideband ISAR Imaging of Maneuvering Targets with Joint High-Order Motion Compensation and Azimuth Scaling," IEEE Transactions on Geoscience and Remote Sensing, vol. 60, pp. 1–21, 2022.

[3] J. Wang, Y. Li, L. Du, M. Song, and M. Xing, "Joint Estimation of Satellite Attitude and Size Based on ISAR Image Interpretation and Parametric Optimization," IEEE Transactions on Geoscience and Remote Sensing, vol. 60, pp. 1–17, Aug. 2021.

[4] Z. Ya, L. Zhang, Y. Cao, and Z. Wu, "Attitude Estimation and Geometry Reconstruction of Satellite Targets Based on ISAR Image Sequence Interpretation," IEEE Transactions on Aerospace and Electronic Systems, vol. 55, no. 4, pp. 1698–1711, Aug. 2019.

[5] N. J. Wang and D. Kasilingam, "Global range alignment for ISAR," IEEE Transactions on Aerospace and Electronic Systems, vol. 39, no. 1, pp. 351–357, Jan. 2003.

[6] D. Zhu, L. Wang, Y.-S. Yu, Q. Tao, and Z. Zhu, "Robust ISAR Range Alignment via Minimizing the Entropy of the Average Range Profile," IEEE Geoscience and Remote Sensing Letters, vol. 6, no. 2, pp. 204–208, Apr. 2009.

[7] W. Ye, Tat Soon Yeo, and Z. Bao, "Weighted least-squares estimation of phase errors for SAR/ISAR autofocus," IEEE transactions on geoscience and remote sensing, vol. 37, no. 5, pp. 2487–2494, Jan. 1999.

[8] S.-H. Lee, J.-H. Bae, M.-S. Kang, C.-H. Kim, and K.-T. Kim, "ISAR autofocus by minimizing entropy of eigenimages," 2022 IEEE Radar Conference (RadarConf22), May 2016.

[9] R. Chen, Y. Jiang, H. Ni, and Y. Zhang, "Spaceborne ISAR Imaging of Space Target With Intra-pulse Motion Compensation Based on Modified Phase Difference," IEEE Geoscience and Remote Sensing Letters, vol. 22, pp. 1–5, 2025.

[10] Y. Liu et al., "Echo Model Analyses and Imaging Algorithm for High-Resolution SAR on High-Speed Platform," IEEE Transactions on Geoscience and Remote Sensing, vol. 50, no. 3, pp. 933–950, Sep. 2011.

[11] L. Zhang, J. Sheng, J. Duan, M. Xing, Z. Qiao, and Z. Bao, "Translational motion compensation for ISAR imaging under low SNR by minimum entropy," EURASIP Journal on Advances in Signal Processing, vol. 2013, no. 1, Feb. 2013.

[12] Deniz Ustun, C. Ozdemir, A. Akdagli, Abdurrahim Toktas, and Mustafa Berkan Bicer, "A powerful method based on artificial bee colony algorithm for translational motion compensation of ISAR image," Microwave and Optical Technology Letters, vol. 56, no. 11, pp. 2691–2698, Aug. 2014.

[13] W. Hu and G. G. Yen, "Adaptive Multiobjective Particle Swarm Optimization Based on Parallel Cell Coordinate System," IEEE Transactions on Evolutionary Computation, vol. 19, no. 1, pp. 1–18, Feb. 2015.

[14] W. Juan and W. Ping, "Optimization of Fuzzy Rule Based on Adaptive Genetic Algorithm and Ant Colony Algorithm," International Conference on Computational and Information Sciences, pp. 359–362, Dec. 2010